Research

New Phytologist

Rethinking the potential productivity of crassulacean acid metabolism by integrating metabolic dynamics with shoot architecture, using the example of *Agave tequilana*

Yu Wang[1], J. Andrew C. Smith[2], Xin-Guang Zhu[3] and Stephen P. Long[1,2,4]

[1]Carl R. Woese Institute for Genomic Biology, University of Illinois at Urbana-Champaign, 1206 W. Gregory Dr., Urbana, IL 61801, USA; [2]Department of Biology, University of Oxford, South Parks Road, Oxford, OX1 3RB, UK; [3]Key Laboratory for Plant Molecular Genetics, Center of Excellence for Molecular, Plant Sciences, Chinese Academy of Sciences, Shanghai, 200031, China; [4]Departments of Plant Biology and of Crop Sciences, University of Illinois at Urbana-Champaign, 505 South Goodwin Avenue, Urbana, IL 61801, USA

Author for correspondence:
Stephen P. Long
Email: slong@illinois.edu

Received: *31 October 2022*
Accepted: *4 June 2023*

New Phytologist (2023) **239:** 2180–2196
doi: 10.1111/nph.19128

Key words: 3-D plant form, bioenergy, crassulacean acid metabolism (CAM) photosynthesis, crassulacean acid metabolism, drought, food security, metabolic model, photosynthesis.

Summary

- Terrestrial CAM plants typically occur in hot semiarid regions, yet can show high crop productivity under favorable conditions.
- To achieve a more mechanistic understanding of CAM plant productivity, a biochemical model of diel metabolism was developed and integrated with 3-D shoot morphology to predict the energetics of light interception and photosynthetic carbon assimilation.
- Using *Agave tequilana* as an example, this biochemical model faithfully simulated the four diel phases of CO_2 and metabolite dynamics during the CAM rhythm. After capturing the 3-D form over an 8-yr production cycle, a ray-tracing method allowed the prediction of the light microclimate across all photosynthetic surfaces. Integration with the biochemical model thereby enabled the simulation of plant and stand carbon uptake over daily and annual courses.
- The theoretical maximum energy conversion efficiency of *Agave* spp. is calculated at 0.045–0.049, up to 7% higher than for C_3 photosynthesis. Actual light interception, and biochemical and anatomical limitations, reduced this to 0.0069, or 15.6 Mg ha^{-1} yr^{-1} dry mass annualized over an 8-yr cropping cycle, consistent with observation. This is comparable to the productivity of many C_3 crops, demonstrating the potential of CAM plants in climates where little else may be grown while indicating strategies that could raise their productivity.

Introduction

The day–night cycle of crassulacean acid metabolism (CAM) is divided conventionally into four phases (Osmond, 1978). Phase I occurs at night when stomatal conductance is high (Males & Griffiths, 2017), and CO_2 is fixed (as bicarbonate) by phospho*enol*pyruvate carboxylase (PEPC) into oxaloacetate (OAA) using PEP generated from storage carbohydrate (Borland *et al.*, 2016). The OAA is then reduced by malate dehydrogenase (MDH) to malate, which is transported into the vacuole and accumulates as malic acid, causing the distinctive nocturnal acidification of the photosynthetic tissues (Winter & Smith, 2022). Phase II occurs in the early morning and represents the transition from nighttime carbon fixation by PEPC to daytime CO_2 assimilation via Rubisco. For most of the light period, during phase III, the stomata are closed while malate is released from the vacuole (Smith *et al.*, 1996; Ceusters *et al.*, 2021) and is decarboxylated in the cytoplasm via either NAD(P)-malic enzyme (NAD(P)-ME) or PEP carboxykinase (PEPCK), releasing CO_2 for assimilation by Rubisco. In this phase, intercellular CO_2 concentrations are dramatically elevated, typically exceeding 0.1% (v/v) but reaching $>2\%$ (v/v) at maximum (Cockburn *et al.*, 1979; Spalding *et al.*, 1979). This should be sufficient to competitively inhibit photorespiratory oxygenation. Stomatal opening may then occur in phase IV in the late afternoon once the stored malate has been exhausted, environmental conditions permitting (e.g. sufficient water availability). In this phase, CO_2 from the atmosphere is assimilated directly by Rubisco, as in C_3 photosynthesis.

Because CAM plants conduct most of their carbon fixation at night, when the ambient temperature is lower and rates of potential evapotranspiration are reduced, they can achieve water savings of 20–80% compared with C_3 or C_4 plants (Nobel, 1991; Borland *et al.*, 2009; Davis *et al.*, 2014). The kinetic properties of PEPC allow CAM plants to maintain a low CO_2 compensation point in the dark (Kluge & Ting, 1978), which further contributes to an elevated water-use efficiency for a given stomatal aperture, as in C_4 plants. For these reasons, CAM plants maintain a strong water-use efficiency advantage over C_3 and C_4 plants in environments with large diel temperature ranges and high daytime water vapor pressure deficits (VPD; Nobel, 1988; Davis *et al.*, 2014). This is reflected in the high proportion of CAM species in the floras of hot semiarid regions (Winter, 1985;

Borland *et al.*, 2009; Ogburn & Edwards, 2010). Such regions account for one-third of global land area and are generally unsuited to C_3 and C_4 crop production (Van Velthuizen, 2007), so CAM crops such as *Agave*, *Opuntia* and *Aloe* could provide a viable alternative land use without irrigation (Cushman *et al.*, 2015; Yang *et al.*, 2015; Davis *et al.*, 2019). Furthermore, engineering the CAM pathway into non-CAM crops has been proposed as an approach for improving WUE whilst maintaining high productivity (Borland *et al.*, 2014; Lim *et al.*, 2019; Schiller & Bräutigam, 2021).

Understanding key mechanistic elements of CAM photosynthesis is essential to guide bioengineering and targeted breeding improvements of the productivity of these crops (Yang *et al.*, 2015; Abraham *et al.*, 2016; Shameer *et al.*, 2018; Burgos *et al.*, 2022). Mathematical modeling has proved valuable in identifying targets for the bioengineering of increased efficiency and sustainability of C_3 and C_4 crops (Zhu *et al.*, 2004, 2007; Wang *et al.*, 2014b, 2021; Kromdijk *et al.*, 2016; Köhler *et al.*, 2017; De Souza *et al.*, 2022), but this approach has been less explored in CAM plants. In fact, due to the time dependence of CAM photosynthesis, kinetic modeling was used in CAM before its application to C_3 and C_4 photosynthesis (reviewed by Morgan & Rhodes, 2002). Comins & Farquhar (1982) predicted the relationship between nocturnal stomatal opening, carbon gain and water loss in CAM plants. Other early kinetic models focused on simulating the daytime vs nighttime phenomena of CAM, such as the diel rhythms of CO_2 uptake and malic acid concentration (Nungesser *et al.*, 1984; Lüttge & Beck, 1992; Blasius *et al.*, 1997, 1998, 1999; Neff *et al.*, 1998; Lüttge, 2000), highlighting malate transport across the tonoplast as a possible regulator of the day/night rhythm of CAM. Owen & Griffiths (2013) developed a system dynamics model of CAM using key biophysical and biochemical parameters related to CO_2 uptake and assimilation, which successfully captured the cardinal features of the diel CAM rhythm. Flux balance models have also been used to predict fluxes in the complete metabolic network of CAM cells with the objective of maximizing phloem loading, as a proxy for growth (Cheung *et al.*, 2014; Shameer *et al.*, 2018; Töpfer *et al.*, 2020). However, none of these models has so far incorporated temperature and light variations or integrated these into the unusual 3-dimensional canopy structures of CAM crops. This is needed to deliver a more complete framework able to predict crop CO_2 assimilation dynamics, long-term productivity and targets for improvement.

Nobel (1984) developed the environmental productivity index (EPI) as a first-order approximation of the effect of environmental factors on net CO_2 uptake of CAM plants, primarily to explain the relative effects of light, temperature and water availability on plant growth. This approach has been used to predict the productivity of a number of CAM species under different climates and regions (Nobel, 2000; Owen & Griffiths, 2014; Niechayev *et al.*, 2019a). Bartlett *et al.* (2014) combined the Farquhar photosynthetic model (Farquhar *et al.*, 1980) with a soil–plant–atmospheric continuum (APAC) model to simulate the carbon and water fluxes of CAM plants, which was later applied to predict the global productivity of *Opuntia ficus-indica* and *Agave tequilana* (Hartzell *et al.*, 2018, 2021). However, these models did not include the effects of canopy structure on light interception and carbon assimilation.

Previous dynamic models of CAM productivity have focused on light-saturated photosynthesis, neglecting the effect of light limitation. Although CAM plants grow in some of the highest light intensities on Earth, their unusual shoot morphology results in significant shading. For example, the flattened cladodes of *Opuntia* spp. and thick leaves of *Agave* spp. have two photosynthetic surfaces separated by a central succulent water-storage tissue. While the upper surface of an *Agave* leaf may be exposed to sunlight for much of the day, the lower surface can be shaded from direct sunlight for long periods. Furthermore, as successive leaves of *Agave* mature, the older leaves at the bottom of the rosette become strongly shaded, particularly toward the broad leaf base (Woodhouse *et al.*, 1980; Nobel & García de Cortázar, 1987). Studies on bromeliad leaves have also shown that carbon assimilation capacity in monocot leaves can exhibit a gradient from base to tip (Popp *et al.*, 2003; Freschi *et al.*, 2010; Chaves *et al.*, 2015). Although CO_2 uptake from the atmosphere may be largely restricted to the nighttime in CAM plants, light interception during the daytime is crucial. This is because it affects not only the rate of concurrent photosynthesis but also the amount of storage carbohydrate that can be synthesized to supply PEP in the following dark period as the substrate for CO_2 capture. Consequently, a productivity model for CAM must take account of potential light limitation by dynamically mapping light on the photosynthetic surfaces of the plant over the course of the day and at different growth stages.

Previous models for C_3 and C_4 crops captured light dynamics by predicting sunlit and shaded canopy portions (e.g. De Pury & Farquhar, 1997). However, this approach is not suitable for most CAM crops because of their canopy architecture, strongly nonrandom leaf distribution and the existence of large gaps between plants in stands of CAM plants through much of the growth cycle. A solution is to capture the 3-D form of the plant and use ray tracing to provide predictions of the dynamic light environment, an approach first applied to *Agave* by Nobel & García de Cortázar (1987). Using rice as an example, Song *et al.* (2013) developed a 3-D canopy reconstruction algorithm, together with a ray-tracing algorithm to predict the light environments at each photosynthetic surface in a crop canopy. This approach allows the development of a systems model of whole-plant CAM photosynthesis despite complex forms by combining a shoot canopy micrometeorological model with a dynamic biochemical model.

Here, an integrated model of crop productivity for *Agave tequilana* F.A.C.Weber was developed. This species was selected because of the extensive field data, including productivity measurements. The genus *Agave* (family Asparagaceae; subfamily Agavoideae) forms a distinctive clade of leaf-succulent CAM plants distributed across the deserts and semi-deserts of the Americas (Gentry, 1982; Nobel, 1988). Many species of *Agave* have been cultivated for centuries for beverages, medicines and fiber (Nobel, 1988; Stewart, 2015;

Pérez-Pimienta *et al.*, 2017). Recent productivity studies and life cycle assessments have emphasized their high yield potential (Yan *et al.*, 2011, 2020; Davis *et al.*, 2014, 2017; Owen *et al.*, 2016). With increasing interest in using marginal land for bioenergy and bioproducts, and possibly for food production (Pérez-Pimienta *et al.*, 2017; Nabhan *et al.*, 2022), the ability to predict potential productivity at different locations will be needed. In particular, bioenergy with carbon capture and geological storage (BECCS) has been highlighted as one of the top options for the removal of atmospheric CO_2 (IPCC, 2023). A challenge is producing biomass whilst avoiding conflict with food and feed production, which CAM biomass crops planted in degraded semidesert regions would address. CAM biomass crops in semideserts could have great value for BECCS, given that these climatic regions often coincide with areas suited to geologic sequestration of CO_2, both in the US and world-wide (Kearns *et al.*, 2017).

Here, a dynamic metabolic model of CAM photosynthesis is integrated into a 3-dimensional shoot architecture model, allowing the prediction of light interception and photosynthetic carbon assimilation in time and space across the entire growth cycle. *Agave tequilana* was chosen as an example since it is a well-studied CAM crop, providing significant parameterization, agronomic and validation data (Nobel & Valenzuela, 1987; Yan *et al.*, 2011; Davis *et al.*, 2019). The current study asks the following questions: (1) How efficient is the crop under typical agronomy over a growth cycle when compared to the maximum predicted assimilation via the CAM pathway? (2) To what extent is CO_2 assimilation light-limited when plant architecture, spacing and sun-angle changes are considered? (3) How do biochemical factors and shoot architecture affect theoretical maximum productivity over an *A. tequilana* growth cycle? Although considered here specifically for *A. tequilana*, the approach developed would be applicable to any CAM plant, where 3-D structure has been captured.

Table 1 Definition of symbols and abbreviations.

Abbreviations	Unit	Description
A	Dimensionless	Leaf absorbance
A_c	μmol m^{-2} s^{-1}	Net rate of canopy photosynthetic CO_2 uptake
A_{i_ad}	μmol m^{-2} s^{-1}	Net rate of photosynthetic CO_2 uptake by a facet on the adaxial surface
A_{i_ab}	μmol m^{-2} s^{-1}	Net rate of photosynthetic CO_2 uptake by a facet on the abaxial surface
C_a	Pa	Atmospheric CO_2 partial pressure
C_i	Pa	Intercellular CO_2 partial pressure
F	Dimensionless	Proportion of absorbed light that does not reach the photosystems
g_s	mol m^{-2} s^{-1}	Stomatal conductance
g_{s_o}	mol m^{-2} s^{-1}	Hypothetical maximum stomatal conductance
HCO_3^-	mM	Bicarbonate
I_2	μmol m^{-2} s^{-1}	Photosynthetic photon flux absorbed by photosystem II
I_t	μmol m^{-2} s^{-1}	Total photosynthetic photon flux
J	μmol m^{-2} s^{-1}	Electron transport rate
J_{max}	μmol m^{-2} s^{-1}	Maximal electron transport rate
Mal_t	mM	Total concentration of malate, including mal^{2-}, $Hmal^-$ and undissociated malic acid
OAA	mM	Oxaloacetate
PEP	mM	Phospho*enol*pyruvate
PPFD	μmol m^{-2} s^{-1}	Photosynthetic photon flux density
S_{ground}	m^2	Ground area occupied by the simulated canopy
S_i	m^2	Surface area of a facet
T_{leaf}	°C	Leaf temperature
T_{ampl}	°C	Average daily temperature amplitude
T_{mean}	°C	Mean daily temperature
V_{max}	μmol m^{-2} s^{-1}	Maximum reaction velocity
W_a	Pa	Ambient atmospheric water vapor pressure
W_i	Pa	Intercellular water vapor pressure
Θ	Dimensionless (0–1)	An empirical curvature factor of the response of net CO_2 uptake to PPFD
ε_i	Dimensionless (0–1)	Efficiency of photosynthetically active light interception
ε_t	Dimensionless (0–1)	Energy conversion efficiency from solar energy to stored chemical energy

Materials and Methods

Development of the whole-plant CAM photosynthesis model

The model takes account of the actual structure and growth of crop stands of *Agave tequilana* F.A.C.Weber and consists of three components: (1) canopy architectural model with ray tracing to determine dynamic light interception; (2) CAM metabolic model; and (3) integration of the metabolic and architectural models. Symbols and abbreviations are summarized in Table 1.

3-D plant model and dynamic light interception of its leaf surfaces using forward ray tracing

The 3-D reconstruction algorithm of Song *et al.* (2013) was adapted to *A. tequilana*, based on the measurements of Nobel & Valenzuela (1987). The angle between overlying leaves was assumed equal to the difference between the angle of the lowest and the vertical, divided by the number of overlying leaves (Supporting Information Methods S1: Eqn MS1.10). Leaves are formed in a whorl, and each successive leaf was assumed to be oriented at 137.5° (Nobel, 1988) beyond its predecessor to minimize overlap (Methods S1: Eqn MS1.11).

Adaxial and abaxial surfaces are separated by a thick layer of nonphotosynthetic water-storage tissue (Smith & Nobel, 1986). They were therefore treated as two independent photosynthetic surfaces; no light was assumed to penetrate from one surface to the other. Both surfaces of every leaf were divided into *c.* 80 triangles, giving high spatial resolution while making the calculations tractable in computational time. Hourly lighting of each facet over the course of the day, taking account of solar angle, shading and reflection within the plant, was simulated by ray tracing, as described previously (Song *et al.*, 2013; Wang *et al.*, 2017; Methods S1: Eqns MS1.1–1.9).

Development of a metabolic model for CAM photosynthesis

Following the procedures and principles of earlier models of C_3 and C_4 photosynthesis (Zhu *et al.*, 2007; Wang *et al.*, 2014a,b), CAM is described here by a system of ordinary differential equations (ODEs). Each ODE calculates the metabolite concentration dynamics ($d[M]/dt$) by numerical integration of the differences between rates of generation (v_{in}) and consumption (v_{out}):

$$\frac{d[M]}{dt} = (v_{in} - v_{out})\frac{1}{Vol} \quad \text{Eqn 1}$$

where Vol is the volume of the compartment containing the metabolite per unit leaf surface area. The major reactions and compartmentation modeled, as shown in Fig. 1, are briefly described below. The complete equations and parameters are given in Supporting Information Methods S2.

Michaelis–Menten equations describe the kinetics of each enzyme-catalyzed step as outlined in previous dynamic models of photosynthetic carbon metabolism (Zhu *et al.*, 2007; Wang *et al.*, 2014b; Fig. 1). The detailed kinetic model is for the nicotinamide adenine dinucleotide phosphate (NADP)-ME-type CAM pathway, since NADP-ME is the predominant decarboxylation enzyme in *Agave* spp. (Dittrich, 1976; Osmond, 1978). Kinetic constants for only a few CAM enzymes were available, notably for phospho*enol*pyruvate carboxylase (PEPC) and NADP-ME (Saitou *et al.*, 1992; Nimmo, 2000). For other enzymes, constants from C_4 plants were substituted (Methods S2: Tables MS2.7–2.8).

Carbon metabolism during the night At night (phase I, Fig. 1), the carbohydrate reserve accumulated during the day generates PEP via glycolysis. In *Agave*, the storage carbohydrate is a mixture of soluble sugars, fructans and starch/glucan (Abraham *et al.*, 2016), but for simplicity it is treated here either as solely starch or soluble hexose (Figs S1, S2, respectively). Thus, 1 glucose (C6) equivalent generates 2 PEP together with 2 NADH, which are quantitatively consumed in the subsequent MDH reaction that synthesizes malate. ATP drives the accumulation of malic acid in the vacuole, as substrate for the tonoplast V-ATPase. The hydrolysis of one ATP can pump 2 H^+ across the tonoplast with one malate^{2-} following passively to balance charge (Smith *et al.*, 1996; Winter & Smith, 2022). Half of the ATP required by the V-ATPase can be supplied by substrate-level phosphorylation and the remainder by mitochondrial oxidative phosphorylation (Lüttge *et al.*, 1981; Shameer *et al.*, 2018). The dark respiration rate was set as 1 μmol m^{-2} s^{-1} based on measured O_2 consumption across a range of C_3 species (Davey *et al.*, 2004), which is consistent with rates observed for CAM plants (Lüttge *et al.*, 1981; Lüttge & Ball, 1987).

The relationship between total vacuolar malate ($[Mal]_{vacu}$), that is, the combined concentration of malate and undissociated malic acid, and vacuolar pH (pH_{vacu}) was assumed to follow the relationship measured in the CAM plant *Kalanchoë*

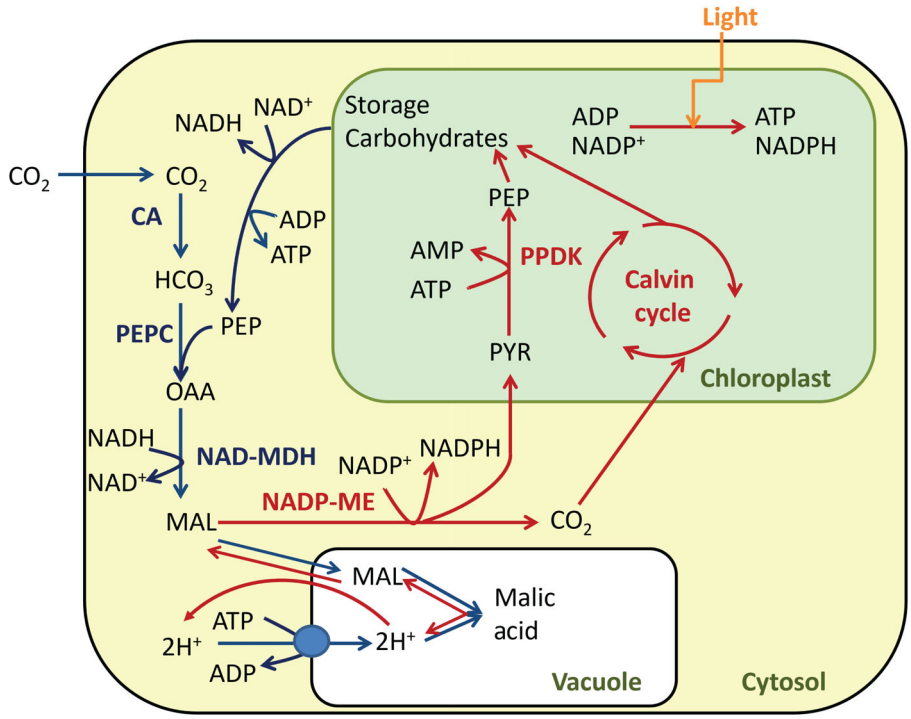

Fig. 1 Metabolites and fluxes represented in the crassulacean acid metabolism (CAM) model (Supporting Information Methods S2). Blue arrows indicate reactions active in the dark; red arrows those active in the day. Daytime malate decarboxylation is shown as catalyzed principally by nicotinamide adenine dinucleotide phosphate (NADP)-linked malic enzyme (NADP-ME), consistent with enzyme activity data for *Agave* spp. (Dittrich, 1976). Enzymes: CA, carbonic anhydrase; MDH, malate dehydrogenase; ME, malic enzyme; PEPC, phospho*enol*pyruvate carboxylase; PPDK, pyruvate, P_i dikinase.

daigremontiana (Lüttge & Smith, 1984; Methods S2: Eqn MS2.40). A minimum pH of 3.5 was specified in the model, such that the rate of malate transport into the vacuole was set at zero at pH ≤ 3.5.

Diel variations of Rubisco and PEPC activities (Methods S2: MS2.3) were set as in Owen & Griffiths (2013), following known patterns of light–dark regulation of these enzymes during CAM (Borland & Griffiths, 1997; Maxwell *et al.*, 1999; Nimmo, 2000).

Carbon metabolism during the day During the day (predominantly during phase III, Fig. 1), CO_2 is released by decarboxylation of malate and is reassimilated via Rubisco into the Calvin-Benson-Bassham (CBB) cycle. The relationship of electron transport rate (J) to photon flux was described by a nonrectangular hyperbola, as in predicting C_3 and C_4 photosynthesis (Ögren & Evans, 1993; von Caemmerer, 2000; Wang *et al.*, 2014a,b; Methods S2: MS2.4). J was used to calculate rates of ATP and NADPH synthesis in photophosphorylation, to drive the CBB cycle.

Assimilation of 1 CO_2 in the CBB cycle ($v_{Rubisco}$) requires 3 ATP and 2 NADPH. Production of 1 PEP via pyruvate, P_i dikinase (PPDK; v_{PPDK}) requires 2 ATP (Winter & Smith, 1996). The rate of ATP concentration change was described as the difference between the rates of generation (v_{ATP_G}) and consumption (Eqn 2). Decarboxylation of malate (v_{NADP_ME}) generates 1 NADPH, which is included in the differential equation describing the rate of NADPH concentration change (Eqn 3).

$$\frac{d[ATP]_{Chl}}{dt} = (v_{ATP\_G} - 2v_{PPDK} - 3v_{Rubisco}) \bullet \frac{1}{Vol_{Chl}} \quad \text{Eqn 2}$$

$$\frac{d[NADPH]_{Chl}}{dt} = (v_{NADPH\_G} + v_{NADP\_ME} - 2v_{Rubisco}) \bullet \frac{1}{Vol_{Chl}} \quad \text{Eqn 3}$$

Stomatal conductance, CO_2 exchange and transpiration Stomatal conductance to CO_2 (g_s) was assumed to be a function of the $[CO_2]$ and water vapor pressure gradients between the leaf intercellular air spaces and air surrounding the leaf (Owen & Griffiths, 2013), paralleling the established phenomenological models for stomatal conductance of C_3 and C_4 leaves (Ball & Berry, 1982; Ball *et al.*, 1987; Collatz *et al.*, 1992):

$$g_s = g_{s\_max} \bullet C_{g_s} \bullet \sqrt{1 - \left(\frac{C_i}{C_a}\right)^2} \frac{W_a}{W_i} \quad \text{Eqn 4}$$

where g_{s_max} is the hypothetical maximum stomatal conductance to CO_2, C_{g_s} is the change factor of stomatal conductance which varied by the time of day and night (Methods S1: MS1.3), C_i is the intercellular $[CO_2]$, C_a is atmospheric $[CO_2]$, W_a is ambient atmospheric water vapor pressure, and W_i is intercellular water vapor pressure. It was assumed that leaf temperature was equal to ambient temperature. Dew point and therefore ambient water vapor pressure were considered constant over the day–night cycle based on meteorological records for Tequila, Mexico (Methods S1: MS1.4). W_i was the saturated water vapor pressure at the temperature of the leaf (Alduchov & Eskridge, 1996). The rate of C_i change (dC_i/dt) was described as the difference between the rate of CO_2 flowing into the intercellular air space and the rate of CO_2 flowing out (Methods S2: Eqn MS2.44).

Temperature response of metabolic reactions The temperature responses of enzyme activities (V_{max}) and affinity for substrate (K_M) were based on those measured for the same enzymes in C_4 species (Boyd *et al.*, 2015; Methods S2: MS2.2). The solubilities of CO_2 and O_2 were calculated using Henry's Law (Methods S2: Eqns MS2.11, 2.12 define the temperature dependence of the constants).

Integrated model of *A. tequilana* canopy photosynthesis

Using the 3-D canopy model and ray-tracing algorithm, hourly photon flux on each facet of each leaf and each surface was predicted and a continuous record in time was obtained by linear interpolation. These predictions together with the diel variation in temperature (Methods S1: MS1.3) were used to calculate CO_2 assimilation, concentrations of CAM pathway intermediates, malate, storage carbohydrate (C6 equivalents) and vacuolar pH at each facet. The rate of accumulation of C6 equivalents is described by Eqn 5. C6 equivalents accumulated during the day as a result of both assimilation of CO_2 via the CBB cycle (1/6 $v_{Rubisco\_C}$) and conversion of PEP derived from malate decarboxylation back to starch or sugars via gluconeogenesis (1/2 v_{PPDK}; Figs 1, S1, S2). At night, C6 equivalents in stored starch, fructan and soluble sugars are consumed to generate PEP (1/2 v_{PEPC}) and supply ATP for malate transport into the vacuole (1/27 v_{PEPC}). Dark respiration (R_d) and photorespiration ($v_{Rubisco\_O}$) also convert some C6 equivalents to CO_2. Thus:

$$\frac{d[C6]_{Cyto}}{dt} = \left(\frac{1}{6}v_{Rubisco\_C} + \frac{1}{2}v_{PPDK} - \frac{1}{2}v_{PEPC} - \frac{1}{27}v_{PEPC} - \frac{1}{6}R_d - \frac{1}{12}v_{Rubisco\_O}\right) \bullet \frac{1}{Vol_{Cyto}} \quad \text{Eqn 5}$$

An intrinsic property of the CAM cycle is that PEP generation at night is limited by the amount of storage carbohydrate accumulated during the previous daytime. A model was run with an arbitrary starting condition, until a 'steady-state' end-of-day amount of storage carbohydrate ($[C6]_{Cyto}$) was achieved after several diel cycles. This quantity was then used as the starting point for the simulations presented here (Fig. S3). Photosynthetic productivity of each leaf surface, that is, net carbohydrate mass gain, was calculated for each 24-h period:

$$A_d = \left([C6]_{Cyto\_i+1} - [C6]_{Cyto\_i}\right) \bullet Vol_{Cyto} \bullet 6MW_{CH_2O} \quad \text{Eqn 6}$$

where $[C6]_{Cyto\_i+1}$ and $[C6]_{Cyto\_i}$ are the C6 concentrations at dusk of day $i+1$ and day i, respectively. Vol_{Cyto} converts the unit

from mM d^{-1} to mmol m^{-2}, and $6 * MW_{CH_2O}$ is the molecular weight of hexose (C6).

Canopy net CO_2 uptake (A_c) was calculated as:

$$A_c = \frac{\sum(A_{d\_i\_ad} \cdot S_i) + \sum(A_{d\_i\_ab} \cdot S_i)}{S_{ground}} \quad \text{Eqn 7}$$

where $A_{d\_i\_ad}$ and $A_{d\_i\_ab}$ are the diel carbohydrate mass gain of adaxial and abaxial sides of a facet, respectively, S_i is the surface area of a facet, and S_{ground} represents the average ground area per plant.

Model solving and application

The system of linked ODEs was numerically integrated to obtain metabolite concentrations via algorithm *ode15s* (MATLAB, 2017). Light distribution over the surfaces, providing the energy to drive the CBB, was predicted by ray tracing using FastTracer, coded in C++ (Song *et al.*, 2013).

Which metabolic and architectural parameters most affected rates of canopy photosynthetic CO_2 uptake was determined by systematic sensitivity analysis. To assess system sensitivity with respect to net canopy CO_2 uptake (A_i), each parameter (p_i, Tables 4, 5) was in sequence decreased by 25% (Δp):

$$SC_p = \frac{A_0 - A_1}{A_0} \bullet \frac{p}{\Delta p} \quad \text{Eqn 8}$$

The original CO_2 uptake rate is A_0, and parameters were sequentially decreased by 25% (Δp) to assess system sensitivity with respect to net canopy CO_2 uptake rate (A_1). SCp represents the fractional change in A per fractional change in p.

Results

Maximum theoretical energy conversion efficiency (ε_t) of CAM

The maximum ε_t of CAM plants was found to range between 0.045 and 0.049, depending on energy cost assumptions and the decarboxylase and storage carbohydrate used (Table 2; Methods S3: Table MS3.2; Fig. S4). These values assume that 90% of all incident photosynthetically active radiation is absorbed and that energy on reaching the reaction centers is used only in the photochemical reduction of CO_2 to storage carbohydrates.

Agave tequilana canopy structure and light interception

Plant architecture of *A. tequilana* was reconstructed for different growth stages (Fig. 2). Incident photon flux is predicted to vary hugely across the photosynthetic surfaces within the plant, as illustrated for a 6-yr-old canopy (Fig. 3). On a clear sky day at 10:00 h, the tips of the leaves receive 2000 µmol m^{-2} s^{-1}, while the lower surfaces near the leaf base can receive < 1% of this (Fig. 3g). The upper surface of the lower leaves (for example facet 40.0.15) may see full sunlight transiently but are in shade for most of the day, while the lower surface is in shade throughout (Fig. 3e).

Table 2 Maximum energy conversion efficiency (ε_t) of C_3, C_4 and crassulacean acid metabolism (CAM) plants.

Photosynthetic type	ATP per CO_2	Nicotinamide adenine dinucleotide phosphate per CO_2	Quantum cost	ε_t
C_3	3	2	8	0.046
C_4 (ME)	5	2	12	0.060
CAM (ME)	7	2	16	0.045/0.045
CAM (PEPCK)	6.25	2	14.5	0.049/0.048

It was assumed that the extra ATP required in the daytime in C_4 plants and CAM plants is generated from cyclic electron transport and that the H^+/ATP ratio is 4. According to the calculation method of Zhu *et al*. (2008), 1 mole quanta has 173.5 kJ energy. One-sixth of a mole glucose (1C carbohydrate unit) contains 477 kJ energy. Maximum energy absorption by photosystems is 37.2%. The costs of photorespiration in both C_4 and CAM are ignored (numbers after '/' considered the cost of photorespiration in Phase IV to be the same as that of C_3 plants, Supporting Information Fig. S12), and respiration is assumed to be 30% of the total net photosynthetic CO_2 uptake for all types of plants. The flux density of photosynthetically active photon interception is assumed as 90% for all photosynthetic types. Details of the calculations are given in Methods S3.

The daily efficiency of light interception (ε_i) averaged over the first 3 yr was just 0.083, but then rose to 0.73 by Year 7. Over the full 8-yr growing cycle, interception efficiency averaged 0.41 (Fig. 4a). As a result, ε_t, the product of ε_i and ε_c, is lowered to just 2.1%.

The predicted interception efficiency of Year 6 (leaf area index of 5.3) increases slightly from 0.67 to 0.73 from the equator to 40° due to the effect of lower average solar elevations (Fig. 4b). ε_i could be raised to 0.88 by increasing planting density to 3906 plants ha^{-1} from the typical planting density of 2500 plants ha^{-1} (Garcia-Moya *et al.*, 2011; Fig. 4c,d).

Prediction and validation of diel leaf CO_2 uptake

Five parameters of our metabolic model are controlled by changes during the diel cycle, that is, Rubisco activity, the malate inhibition constant of PEPC, stomatal conductance and malate transport into and out of the vacuole (Fig. 1; Methods S2: MS2.3). Compared with measured patterns of CO_2 assimilation for different *Agave* species, the model successfully captured the four phases of the CAM cycle in duration and magnitude of flux (Fig. 5a,b), providing strong validation of the model. The predicted late-afternoon Phase IV was accentuated by a simulated 50% elevation of Rubisco activity, showing this to be a key limitation in this phase and in Phase II (Fig. 5b). The response of predicted net diel CO_2 uptake to total incident photosynthetic photon flux matched measured values closely (Fig. 5c).

Sensitivity analysis showed strong effects of varying maximum stomatal and mesophyll conductances, as well as the assumed minimum vacuolar pH, and maximum activities of both PEPC

New Phytologist

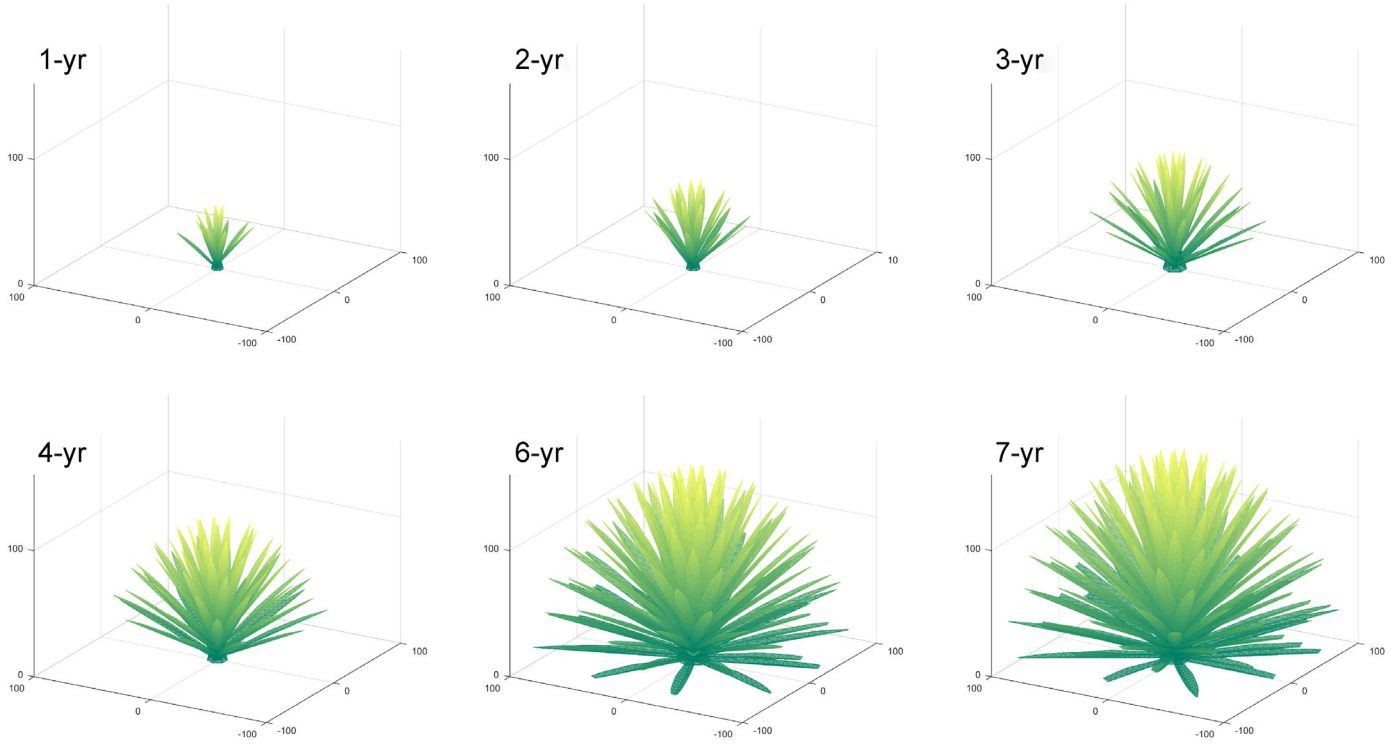

Fig. 2 Reconstructed shoot architecture of an *Agave tequilana* plant following the rules of the structural model through 7 yr of growth developed from prior measurements (Nobel & Valenzuela, 1987; Table 3). The color scheme is simply to depict height above the ground.

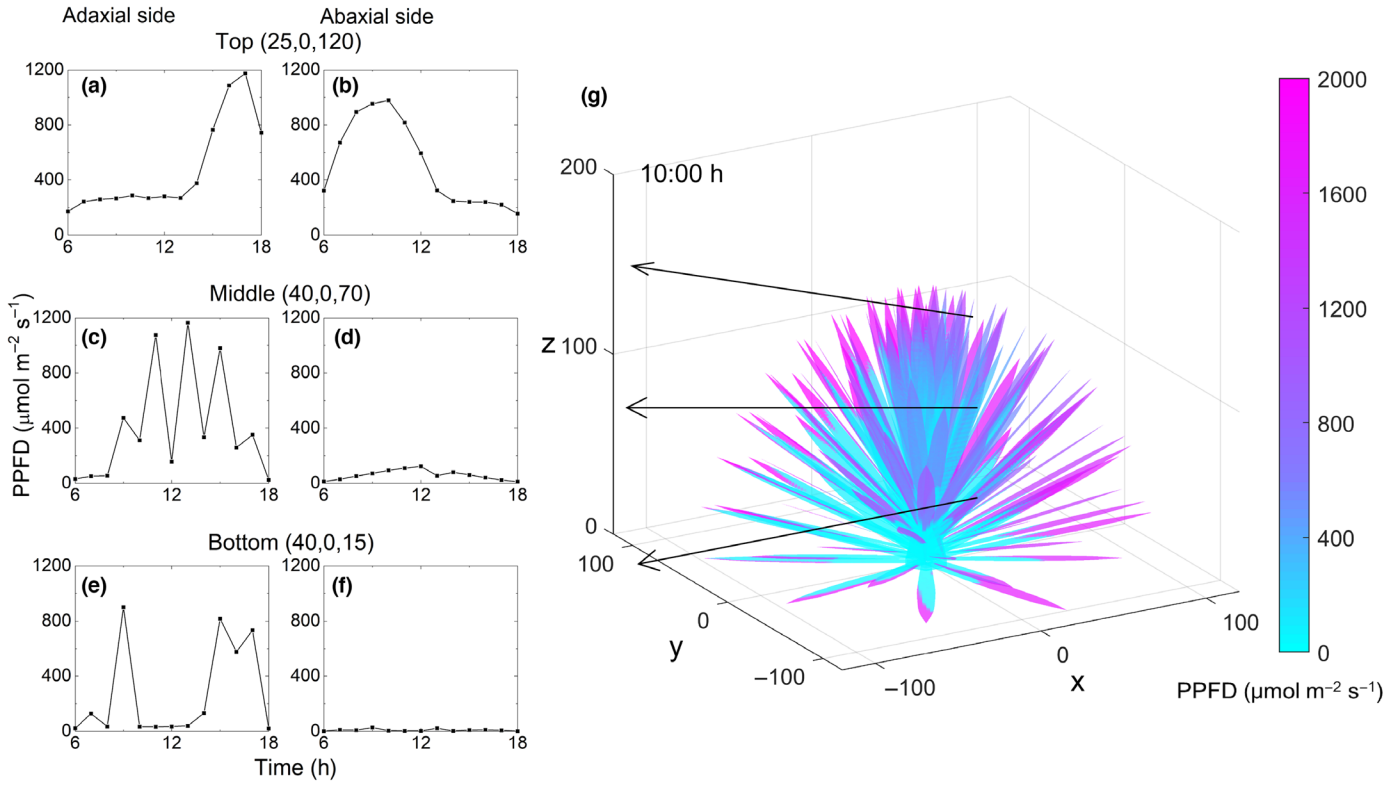

Fig. 3 Diurnal photosynthetically active photon flux density (PPFD) absorption of a single leaf facet on each of the adaxial (a, c, e) and abaxial (b, d, f) surfaces in the top (a, b), middle (c, d) and bottom (e, f) of the *Agave tequilana* canopy are shown on the left-hand side. The coordinate (*x*, *y*, *z*) of the centroid of the leaf facet is noted in parentheses for each height. The simulation is for June 2022 at Tequila, Jalisco, Mexico (20.88°N, 103.83°W). (g) The predicted light environment inside an *A. tequilana* canopy at 10:00 h on the same day.

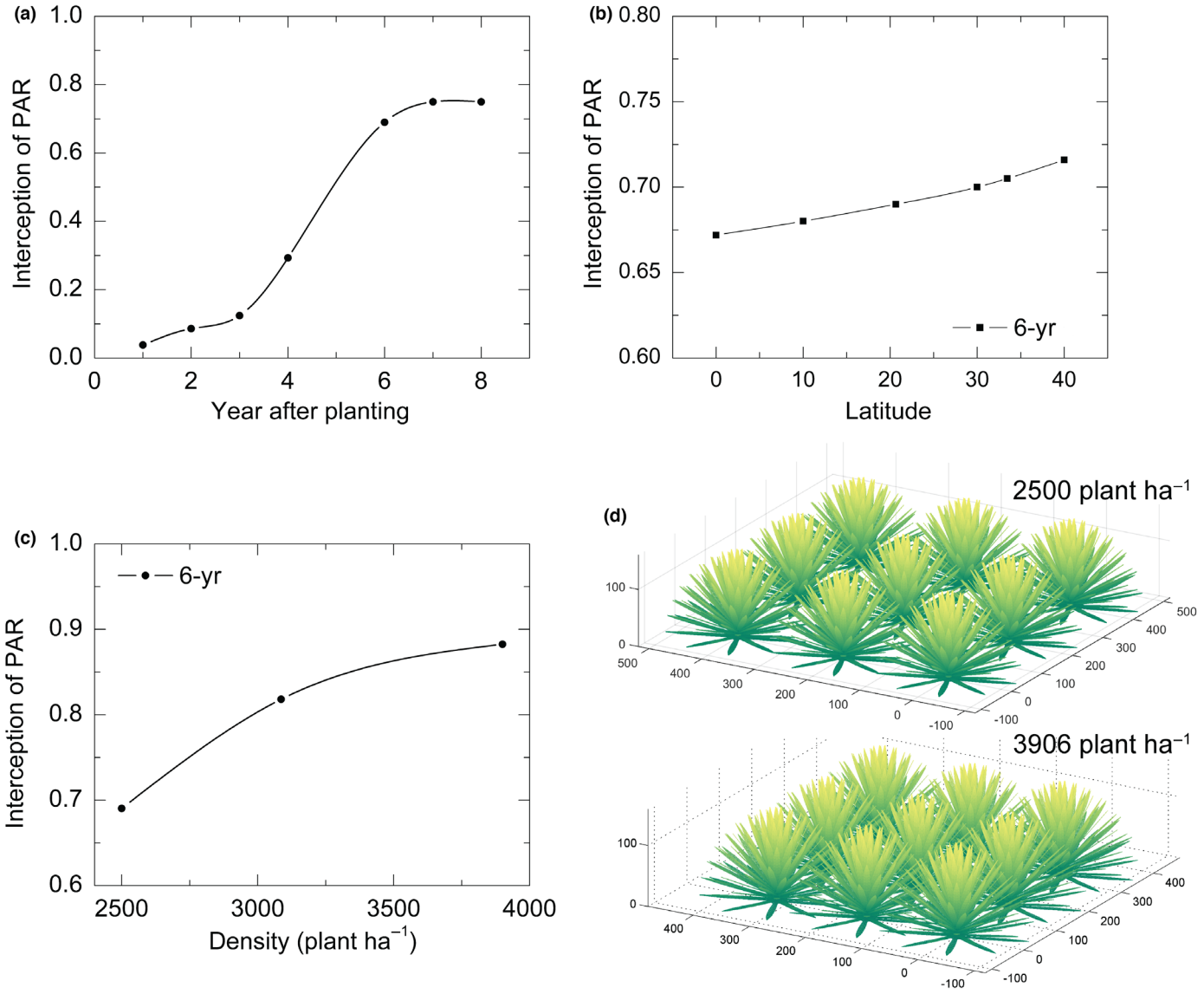

Fig. 4 Canopy light interception with age, density and location of the stand. (a) Proportion of available photosynthetically active photon flux density (PPFD) intercepted each year over the 8-yr growth cycle, assuming a planting density of 2500 ha^{-1} at Tequila, Mexico, on June 2022. (b) The proportion of available PPFD intercepted by a 6-yr-old *Agave tequilana* canopy of leaf area index (LAI) 5.3 and planting density of 2500 ha^{-1} with latitude. (c) As for (a), but with a mature *A. tequilana* canopy with varied plant density. The proportion of PPFD intercepted by a 6-yr-old *A. tequilana* canopy, as affected by planting density. (d) The canopy structure of *A. tequilana* with two planting densities: 2500 ha^{-1} (a plant spacing of 2 m within and between rows) and 3906 ha^{-1} (spacing of 1.6 m). LAI was calculated based on the total area of both sides of all leaves. The color scheme is simply to depict height above the ground.

and vacuolar malate transport. These had the greatest effects on CO_2 assimilated at night in Phase I (Fig. S5). Rubisco activity (Fig. 5b), the assumed minimum pH in the vacuole, and PEPC activity at night exerted strong control over malate availability and hence the duration of Phase III (Fig. S5c,e,f). Conversely, lower Rubisco activity may result in failure to utilize all the malate accumulated during the previous night before the next phase (Fig. S5e). While the results show little increase in nocturnal CO_2 uptake with increased PEPC, large losses result from a decrease in PEPC (Fig. S5). Lowering temperature below a 24-h average of 15°C substantially decreases CO_2 uptake from the atmosphere in both Phase I and Phase IV (Fig. 6).

Factors controlling the total canopy carbon gain of an *A. tequilana* canopy

When photosynthesis of each leaf facet of the canopy is taken into account in the 8-yr growth cycle of *A. tequilana* in Tequila, Mexico (Fig. 7), the efficiency with which the available photosynthetically active radiative energy is converted into chemical energy in the form of biomass is just 0.0069. The annual surface photosynthetically active radiation received at Tequila was taken as 3600 MJ m^{-2}, calculated from the annual average irradiation of 5.7 kWh m^{-2} d^{-1} at nearby Guadalajara (Díaz-Torres *et al.*, 2017), and assuming that PAR is 48.7% of total

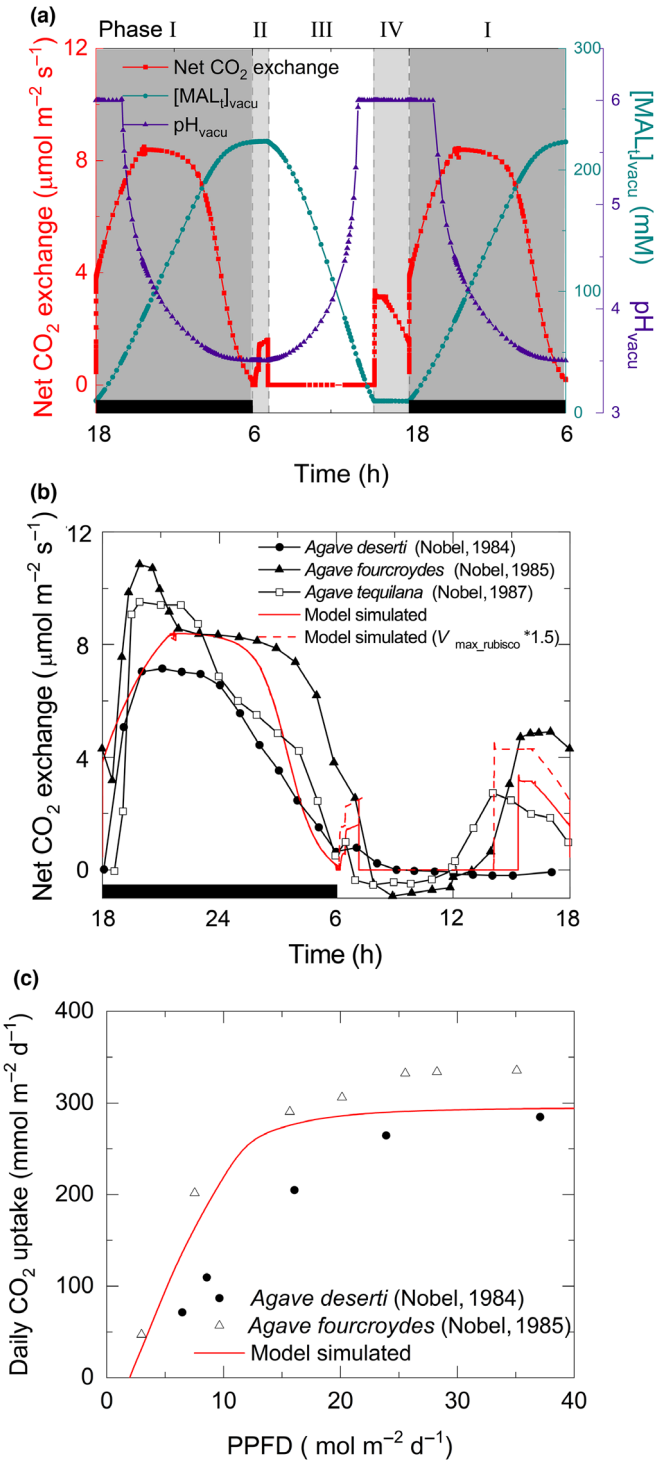

Fig. 5 Modelled and measured diel changes in CO_2 uptake. (a) Simulated diel changes in leaf net CO_2 uptake, total vacuolar malate concentration ($[MAL_t]_{vacu}$) and vacuolar pH. (b) Simulated diel net CO_2 uptake rate across the course of a day in which the accumulated photosynthetic photon flux density is 50 mol m^{-2} d^{-1} (red line). The dashed red line is the simulated net CO_2 uptake rate with a 50% increase in Rubisco activity ($V_{max\_Rubisco}$). Triangles, open circles and squares with black lines are measured rates from Nobel (1984, 1985, 1988). (c) Predicted daily net CO_2 uptake vs photosynthetically active radiation (red line). Closed circles and open triangles are the measured daily assimilation values of Nobel (1984, 1985). The simulations are for a constant temperature of 25°C, which is close to the average of Tequila, Mexico. The black bar along the *x*-axis of (a, b) indicates the duration of darkness (night).

irradiation. Assuming a dry biomass energy content of 16 MJ Mg^{-1}, the efficiency of 0.0069 would result in a productivity of *c.* 1.56 kg m^{-2} yr^{-1}, or 15.6 Mg ha^{-1} annualized over the 8-yr growth cycle. This results from the slow rate at which the *A. tequilana* expands to cover the ground after planting.

To assess the impact of latitude and temperature in desert regions, A_c for a mature (6-yr-old) canopy was assessed for both Phoenix, Arizona, in the USA and Tequila, Jalisco Mexico, using recorded local monthly average temperatures (Fig. 8). Although net carbohydrate gain was similar at both locations in the summer, it was zero for Phoenix in the winter months and also substantially lower in the early spring and late autumn than during the summer months. The predicted productivity of a hypothetical 6-yr plantation was 20.9 Mg ha^{-1} in Phoenix and 28.5 Mg ha^{-1} in Tequila, assuming an LAI of 5.3 at both locations.

Despite being in a high-light environment, the dense packing of thick leaves in the rosette and distribution of half of the photosynthetic apparatus on the abaxial surface results in significant light limitation in *Agave*. This shading is no doubt critical for lowering temperatures and in turn cuticular water loss. However, in Year 1, taking account of light in all daylight hours, 69% of the photosynthetic surface is light-limited, based on assimilation rates < 0.9 of light-saturated rate, rising to 92% by Year 6.

Varying biochemical and anatomical parameters in the sensitivity analysis from 0.25- to 1.75-fold showed that, at the canopy level, Rubisco and minimum vacuolar pH shared the highest control coefficients for total daily canopy mass gain (A_c) during early growth (simulated Year 1). However, by Year 6, Rubisco became dominant (Tables 4, 5; Figs S6–S9).

A_c is linearly related to leaf area index (LAI) in the first 4 yr, approaching an optimum LAI of *c.* 6–7 in Year 6 and 7 (Table 5; Fig. S9a–f). In the canopy, the leaf angle to the vertical progressively increases from top to bottom. The predicted optimal angle of this lowest (oldest) leaf increases with canopy size (Table 5; Fig. S9g–l). A_c showed little sensitivity to leaf reflectance during the first years of growth, but increased reflectance increased A_c in the later years of the crop growth cycle by increasing light at the abaxial surfaces toward the leaf bases (Table 5; Fig. S9m–r). Simulated water-use efficiency (WUE) averaged over 8 yr was *c.* 5 mmol$[CO_2]$ mol$[H_2O]^{-1}$, or 8 g kg^{-1}, showing relatively little sensitivity to LAI, a small increase with leaf reflectivity in later years, but a strong sensitivity to maximum leaf angle (Fig. S9).

Discussion

To explore factors limiting the productivity of CAM plants, a whole-shoot photosynthesis model was developed. This integrated a new kinetic model of carbon assimilation in CAM with

Table 3 Parameters used to construct the 3-D canopy photosynthesis model for *Agave tequilana*.

Parameter	1-yr	2-yr	3-yr	4-yr	6-yr	7-yr	References
Number of leaves	13	22	41	61	114	126	Nobel & Valenzuela (1987)
Leaf length (cm)	41	57	76	90	121	129	Nobel & Valenzuela (1987)
Leaf width (cm)	4.52	5.6	5.33	7.73	9.78	10.09	Calculated based on leaf area and length
Leaf area (m^2 $plant^{-1}$)	0.38	1.09	2.58	6.6	21.14	25.50	Nobel & Valenzuela (1987)
Maximum leaf angle (°)	57	57	69	75	86	86	Assumed

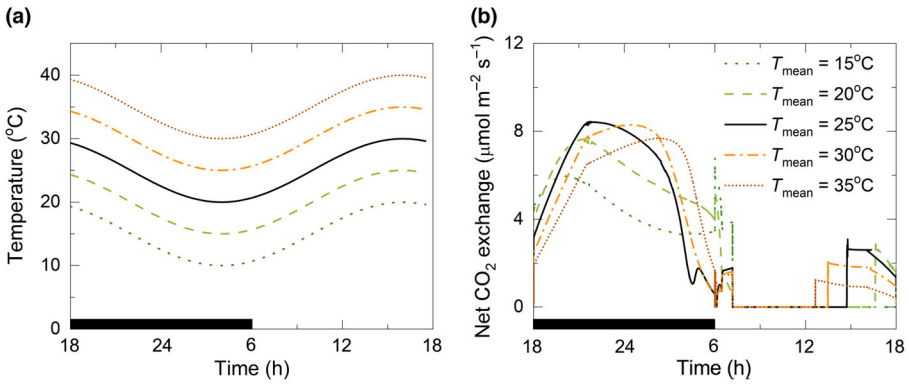

Fig. 6 Influence of leaf temperature on simulated leaf net CO_2 uptake. (a) Simulated diel courses of leaf temperature with 24-h means of 15, 20, 25, 30, or 35°C. (b) The corresponding predicted diel courses of leaf net CO_2 uptake rate. The cumulative PPFD at all temperatures was 50 mol m^{-2} d^{-1}. The black bar along the *x*-axis indicates night.

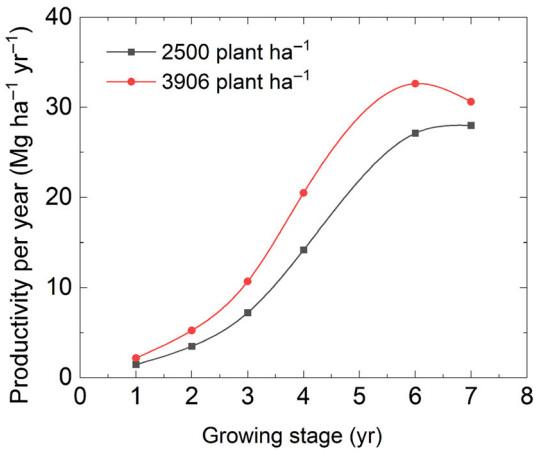

Fig. 7 Canopy carbon accumulation rate of *Agave tequilana* simulated for successive years of growth as depicted in the structural model (Fig. 1) for Tequila, Mexico. The simulation in each case was extrapolated from June 2022. Planting densities were 2500 and 3906 plants ha^{-1}, respectively. The productivity per year was calculated assuming the average daily carbon accumulation for each yr is 74% of that in June (Fig. 8b).

a 3-D canopy architectural model and ray-tracing algorithm to predict temporal and spatial light distribution. In turn, CO_2 assimilation in time and space across the 3-D structure of the shoot was predicted (Figs 2–4). Using *Agave tequilana*, the model predicted the light distribution and net carbon assimilation of the crop over its 8-yr cultivation cycle. Predicted monthly carbon gain and annual productivity were comparable with biomass measurements and eddy covariance studies of *A. tequilana* crops in Mexico (Fig. 8; Nobel, 1988; Owen *et al.*, 2016). The model successfully recapitulated the observed daily patterns of net CO_2 exchange, malic acid content and vacuolar pH in *Agave* through the four phases of CAM (Fig. 5a,b; Neales, 1973; Nobel, 1984, 1985, 1988; Holtum & Winter, 2014; Winter *et al.*, 2014) and provided a good fit to the observed relationship between net diel CO_2 uptake and total incident photosynthetic photon flux (Fig. 5c; Nobel, 1984, 1985).

New features of the CAM canopy photosynthesis model

Our model incorporates new features compared with previous dynamic models. First, the empirically observed relationship between vacuolar pH and malic acid concentration was used to simulate diel changes in vacuolar pH. This enabled regulation of metabolism by vacuolar pH, in which no further net import of malate into the vacuole could occur at night once the minimum pH value (in this case pH 3.5) was reached. In practice, this can correspond to the time at which the pool of storage carbohydrate has been exhausted, so the relative importance of these

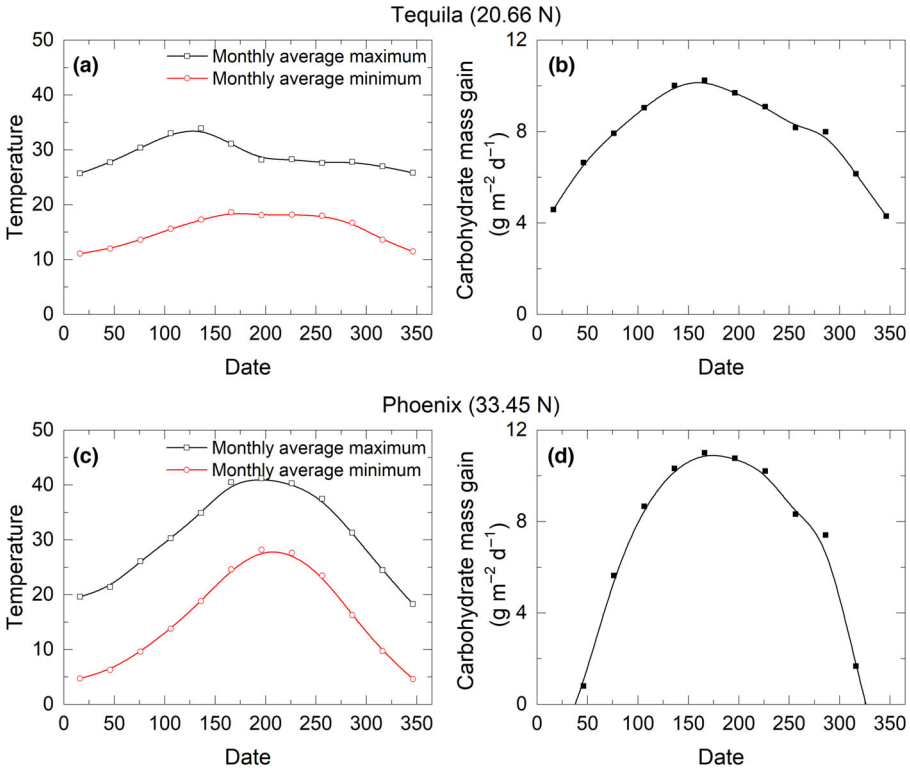

Fig. 8 Model-predicted daily carbon accumulation of a mature *Agave tequilana* canopy (assuming a constant leaf area index of 5.3; as depicted in Fig. 1) over the course of 1 yr in (a, b) Tequila, Mexico and (c, d) Phoenix, USA. Planting density was 2500 plants ha^{-1}. The monthly average maximum and minimum temperatures are shown as black and red lines, respectively (a, c).

limitations to total nocturnal CO_2 fixation would merit further investigation. Second, stomatal conductance is regulated by atmospheric and intercellular CO_2 concentration. Many studies have demonstrated a phenomenological linkage between atmospheric or intercellular CO_2 concentrations (c_i) and stomatal conductance (g_s) in C_3, C_4 and CAM plants, although mechanistically this results, most likely, from co-varying signal(s) (summarized by Morison, 1987). The possible linkage between c_i and g_s, and corresponding CO_2 uptake rate (A), still needs further elucidation, especially in relation to processes responsible for the characteristic inverse stomatal rhythm of CAM plants (Males & Griffiths, 2017). Third, temperature effects are accounted for through effects on enzyme activity, CO_2 solubility and saturated water vapor pressure (Methods S2: MS2.2). This enables the model to predict the performance of CAM photosynthesis in different temperature regimes that characterize the habitats in which CAM plants are found or might be being considered for planting. And fourth, the balance of energy (ATP and NADPH) production and consumption is explicitly included, so the response of A to PPFD can be accurately simulated in real time.

Given our imperfect understanding of CAM, the current model inevitably has limitations. For instance, it employs a phenomenological prediction of g_s and incorporates circadian-regulated parameters to obtain the four phases of CAM photosynthesis (Eqn 4; Methods S2: MS2.3; Fig. S10). Furthermore, we have not performed a continuous simulation for the entire growth period. Nevertheless, this model provides a framework for future extension both with new data and for other CAM species. To enhance the accuracy of model predictions, a significant amount of biochemical and physiological data, including systematic anatomical, physiological, biochemical and signal transduction datasets for the target species will be critical. Though the current model is parameterized for *A. tequilana*, it can be easily adapted for other CAM species of agronomic importance, such as pineapple (*Ananas comosus* (L.) Merr.).

While simplified equations that dynamically partition sunlit and shaded leaf area have proven very effective for C_3 and C_4 crops (De Pury & Farquhar, 1997), the form of most CAM crops violates the assumptions of these models. The ray-tracing method used here for *Agave* would be readily applicable to other CAM plants, as has been demonstrated for *Opuntia* spp. by Nobel (1988), despite their very different shoot morphology. The present model could also be used to contrast the potential benefit of water saving by CAM plants, or facultative CAM plants, for example, *Talinum triangulare* (Brilhaus *et al.*, 2015), with typical C_3 or C_4 plants. Finally, with increasing interest in engineering C_3 plants to perform inducible CAM photosynthesis in response to drought (Borland *et al.*, 2014; Yang *et al.*, 2015; Lim *et al.*, 2019; Niechayev *et al.*, 2019b; Schiller & Bräutigam, 2021), our model provides a framework for testing different engineering options for CAM biodesign.

In the past few years, technical advances have provided ever-increasing numbers of CAM genomes, transcriptomes and metabolomes (Ming *et al.*, 2015; Wai *et al.*, 2017; Yang *et al.*, 2017; Ceusters *et al.*, 2019). To extract useful information from large amounts of 'omics data, computational modeling approaches are

Table 4 Biochemical and physiological parameters used in the model of *Agave techilana* and their sensitivities with respect to daily total canopy net photosynthetic CO_2 uptake rate.

Parameter	Default value	Sensitivity coefficient		
		Year 1	Year 3	Year 6
g_s	0.1 mol m^{-2} s^{-1}	0.06	0.05	0.05
g_m	0.1 mol m^{-2} s^{-1}	0.02	0.02	0.02
V_{max_PEPC}	35 μmol m^{-2} s^{-1}	0.01	−0.01	−0.03
$V_{max\_Rubisco}$	30 μmol m^{-2} s^{-1}	0.30	0.36	0.57
$V_{max\_MAL\_in}$	80 μmol m^{-2} s^{-1}	0.04	0.04	0.05
$[pH]_{vacu\_min}$	pH = 3.5	0.27	0.21	0.15

Simulation for June 2022 at Tequila, Mexico (latitude 20.66°N). Each parameter was decreased by 25% to assess system sensitivity with respect to net canopy CO_2 uptake rate (Eqn 8).

Table 5 Sensitivity of different shoot architectural parameters of *Agave tequilana* to daily total canopy net photosynthetic CO_2 uptake rate.

Parameter	Growing stage (yr)	Default value	Sensitivity coefficient
Leaf area index (m^2 m^{-2})	1	0.09	0.89
	2	0.27	0.95
	3	0.64	0.86
	4	1.65	0.86
	6	5.29	0.58
	7	6.37	0.46
Maximum leaf angle (°)	1	57	0.12
	2	57	0.29
	3	69	0.16
	4	75	0.55
	6	86	0.61
	7	86	0.62
Leaf reflectance	1	0.1	−0.01
	2	0.1	0.04
	3	0.1	0.07
	4	0.1	0.13
	6	0.1	0.26
	7	0.1	0.29

Simulation was for June 2022 at Tequila, Mexico (latitude 20.66°N). Each parameter was decreased by 25% to assess system sensitivity with respect to net canopy CO_2 uptake rate (Eqn 8).

increasingly important (Shameer *et al.*, 2018; Chomthong & Griffiths, 2020; Burgos *et al.*, 2022). With the methods of model integration we developed previously (Kannan *et al.*, 2019; Shameer *et al.*, 2022), our CAM model has the potential to interface with transcriptome data, gene regulatory networks and metabolic models based on flux balance analysis (Cheung *et al.*, 2014; Shameer *et al.*, 2018; Töpfer *et al.*, 2020). This will enable the exploration and assessment of the potential of CAM crops of varying forms in a more comprehensive way, identifying potential targets for yield improvement and contributing to CAM biodesign. Recent progress in implementing RNAi and CRISPR/Cas9 approaches in investigating the regulation and expression of CAM photosynthesis (Dever *et al.*, 2015; Liu *et al.*, 2019; Boxall *et al.*, 2020) has opened a feasible way to test and realize such model predictions.

How efficient can the crop be over a growth cycle by comparison with the predicted theoretical maximum of CAM?

ε_t is the proportion of solar energy incident on a unit area of ground, accumulated in the crop as biomass. The theoretical maximum ε_t of *Agave* spp. (NADP-ME CAM) was 0.045, similar to C_3 photosynthesis (Table 2; Methods S1: Table MS3.2; Fig. S4). Two factors may slightly reduce this calculated efficiency of *Agave tequilana* crops. First, it does not account for photorespiration. However, photorespiration has to result if Rubisco is fixing CO_2 directly from the atmosphere, as in Phase IV. Indeed, experimental observations show that *c.* 25% of diel C fixation in *Agave* can occur in Phase IV under well-watered conditions (Winter *et al.*, 2014). This will vary with temperature and the duration of Phase IV. Second, our calculation of NAD(P)-ME CAM assumes starch as the storage carbohydrate, releasing glucose monomers via the phosphorolytic pathway in Phase I (Fig. S1). However, sucrose and fructans are significant components of the storage carbohydrate pool in *Agave* (Abraham *et al.*, 2016). Their remobilization incurs slightly higher energy costs. In the flux balance analysis of Shameer *et al.* (2018), the theoretical energy conversion efficiency using sucrose or fructans as the source of PEP is 0.945 or 0.832 of that of starch, respectively.

The achieved ε_t in the first 3 yr of a field crop of *A. tequilana* under typical agronomy is much lower than that of annual C_3 and C_4 crops (Table 2). Light interception is initially low due to slow ground coverage after planting. Our results indicate that average light interception over the entire growing cycle is only 41% at a typical planting density for *A. tequilana* of 2500 plants ha^{-1}, reaching *c.* 75% in Year 7 (Fig. 4a), whereas the crop only absorbs 8.3% of total incident light in its first 3 yr (Fig. 4a). Thus, the ε_t of *A. tequilana* over the whole growth cycle is only 0.021%. Although this is much lower than the theoretical maximum value of either C_3 or C_4 plants (Table 2), it is comparable to the realized ε_t of C_3 and C_4 crops in the field. For example, the realized ε_t of wheat and rice is *c.* 0.02 (Slattery & Ort, 2015).

Arid and semiarid regions account for about one-third of the global land area (5 billion ha). These are regions where most C_3 and C_4 crops cannot grow or are limited to short and unpredictable rainy seasons (Van Velthuizen, 2007). These regions have been expanding and are predicted to account for > 40% of global land by 2100 (Huang *et al.*, 2016; Prăvălie, 2016). Using *A. tequilana* as a well-studied example, the peak productivity of *Agave* has been claimed to be as high as 50 Mg dry biomass ha^{-1} yr^{-1}, which with a sugar content of *c.* 27–38% (w/w) could produce an ethanol yield of up to 14 000 l ha^{-1} (Borland *et al.*, 2009). This could double with high-yielding cultivars and appropriate management (Yan *et al.*, 2011). Theoretically, if 0.14% of the world's arid and semiarid regions were used to cultivate *A. tequilana*, and assuming only its nonstructural carbohydrates are used to produce ethanol, the ethanol productivity could be as high as 97 billion liters, equivalent to the total amount of ethanol produced globally in 2021 (RFA, 2021).

What proportion of the photosynthetic surface is light-limited in the canopy?

Although CAM in desert species might be considered light-saturated for most of the day, ray tracing shows a very significant part of the photosynthetic surface to be light-limited in *A. tequilana*. Nobel & García de Cortázar (1987) also described this effect for *Agave* species, noting that light limitation was especially pronounced in the lower leaves with plant age. Consistent with measured values for *A. tequilana*, Fig. 5c predicts that a PPFD of 20 mol m^{-2} d^{-1} would be needed to utilize all malate accumulated in the previous night. However, on a clear sky summer day, 55% of the photosynthetic surfaces in Year 1 and 85% of the surfaces by Year 7 would receive < 20 mol m^{-2} d^{-1}. Furthermore, *Agave* species often have concavely curved leaves, which would result in an even larger proportion of the photosynthetic surfaces being light-limited, especially on the adaxial surface (Fig. S10).

Are there realistic opportunities to increase the energy conversion efficiency (ε_t) of *Agave* spp.?

Failure of *A. tequilana* to intercept much of the available light in the earlier years of its 8-yr growth cycle is due to the slow closure of the canopy (Fig. 4a). Our simulation indicated that increasing planting density to 3906 plants ha^{-1} would increase light interception by *c.* 27.5% (Fig. 4c), increasing productivity up to 20.3% (Fig. 7).

At standard planting densities, interception and productivity approach a plateau of *c.* 27 Mg ha^{-1} yr^{-1} in Year 6 (Fig. 7), a high productivity comparable to the best C_4 and C_3 crops. However, this is when the stem base is ready for harvest, and the cycle recommences. This efficiency may, however, be maintained in *Agave* species grown for fiber, such as sisal (*Agave sisalana* Perrine) and henequen (*Agave fourcroydes* Lem.), which may have a growth cycle of 15+ yr. Here, lower leaves can be harvested to maintain a constant canopy size, once near canopy closure is achieved (Purseglove, 1972; Nobel, 1988). If the Year 6 productivity was similar to *A. tequilana*, but maintained for a further 10 yr, the annualized conversion efficiency would increase to 0.009 and the biomass yield to 20.3 Mg ha^{-1} yr^{-1}. This exceeds the yields of the temperate C_4 perennial biomass crop *Panicum virgatum* (switchgrass) and is comparable to the even more productive *Miscanthus* × *giganteus* (Beale & Long, 1995; Arundale *et al.*, 2014).

With the present model, we systematically evaluated potential manipulations that can be performed to improve the carbohydrate mass gain of the crop, specifically the architectural and biochemical parameters. Of the factors that may hold promise for future crop improvement, leaf area index (LAI) and maximal leaf angle are the two most important canopy architectural parameters. Variations in these have major impacts on canopy CO_2 uptake due to altered light interception and distribution in the canopy (Table 5; Fig. S9). Leaf reflectance does not influence canopy productivity in the early growing stages, but it becomes a major factor in mature *A. tequilana* plants, as higher leaf reflectance can increase carbon gain by *c.* 20%. Rubisco was predicted to be the most important enzyme controlling *A. tequilana* canopy photosynthesis throughout the entire growing season. Minimum vacuolar pH, which may ultimately limit malate storage capacity in Phase I, also had a high control coefficient over canopy photosynthesis in the early growth stages (Table 4; Figs S6–S8).

This study has developed a means to integrate the unique 3-D structures and metabolism of CAM crops to predict ways to improve productivity through agronomic, plant structural and metabolic modification, using the example of *A. tequilana*. It strengthens proposals to further develop and utilize CAM on the large global tracts of degraded semidesert or arid land that are not accessible to the majority of staple food crops.

Acknowledgements

Financial support is acknowledged from the Oxford Martin School (Dryland Bioenergy program; JACS) and the Newton–Abraham Professorship funds (SPL) at the University of Oxford. We thank Bethany Holland, Edward B. Lochocki, Yi Xiao, Jeff Hansen and Elena A. Pelech for their comments and advice on this manuscript.

Competing interests

None declared.

Author contributions

SPL, JACS, X-GZ and YW designed the study. YW performed computational analysis. SPL, JACS, X-GZ and YW wrote the paper.

ORCID

Stephen P. Long https://orcid.org/0000-0002-8501-7164
J. Andrew C. Smith https://orcid.org/0000-0001-9188-0258
Yu Wang https://orcid.org/0000-0002-6951-2835
Xin-Guang Zhu https://orcid.org/0000-0002-4435-130X

Data availability

Code that supports the findings of this study is available at GitHub (https://github.com/yuwangcn/CAM-model).

References

Abraham PE, Yin H, Borland AM, Weighill D, Lim SD, De Paoli HC, Engle N, Jones PC, Agh R, Weston DJ *et al.* 2016. Transcript, protein and metabolite temporal dynamics in the CAM plant *Agave*. *Nature Plants* **2**: 16178.

Alduchov OA, Eskridge RE. 1996. Improved Magnus form approximation of saturation vapor pressure. *Journal of Applied Meteorology* **35**: 601–609.

Arundale RA, Dohleman FG, Heaton EA, McGrath JM, Voigt TB, Long SP. 2014. Yields of *Miscanthus* × *giganteus* and *Panicum virgatum* decline with stand age in the Midwestern USA. *Global Change Biology Bioenergy* **6**: 1–13.

Ball JT, Woodrow IE, Berry JA. 1987. A model predicting stomatal conductance and its contribution to the control of photosynthesis under different environmental conditions. In: Biggens J, ed. *Progress in photosynthesis research, vol. IV*. Dordrecht, the Netherlands: Martinus Nijhoff Publishers, 221–224.

Ball TJ, Berry JA. 1982. The C_i/C_s ratio: a basis for predicting stomatal control of photosynthesis. *Carnegie Institution of Washington Year Book* **81**: 88–92.

Bartlett MS, Vico G, Porporato A. 2014. Coupled carbon and water fluxes in CAM photosynthesis: modeling quantification of water use efficiency and productivity. *Plant and Soil* **383**: 111–138.

Beale CV, Long SP. 1995. Can perennial C_4 grasses attain high efficiencies of radiant energy conversion in cool climates? *Plant, Cell & Environment* **18**: 641–650.

Blasius B, Beck F, Lüttge U. 1997. A model for photosynthetic oscillations in crassulacean acid metabolism (CAM). *Journal of Theoretical Biology* **184**: 345–351.

Blasius B, Beck F, Lüttge U. 1998. Oscillatory model of crassulacean acid metabolism: structural analysis and stability boundaries with a discrete hysteresis switch. *Plant, Cell & Environment* **21**: 775–784.

Blasius B, Neif R, Beck F, Lüttge U. 1999. Oscillatory model of crassulacean acid metabolism with a dynamic hysteresis switch. *Proceedings of the Royal Society of London B: Biological Sciences* **266**: 93–101.

Borland AM, Griffiths H. 1997. A comparative study on the regulation of C_3 and C_4 carboxylation processes in the constitutive crassulacean acid metabolism (CAM) plant *Kalanchoë daigremontiana* and the C_3–CAM intermediate *Clusia minor*. *Planta* **201**: 368–378.

Borland AM, Griffiths H, Hartwell J, Smith JAC. 2009. Exploiting the potential of plants with crassulacean acid metabolism for bioenergy production on marginal lands. *Journal of Experimental Botany* **60**: 2879–2896.

Borland AM, Guo H-B, Yang X, Cushman JC. 2016. Orchestration of carbohydrate processing for crassulacean acid metabolism. *Current Opinion in Plant Biology* **31**: 118–124.

Borland AM, Hartwell J, Weston DJ, Schlauch KA, Tschaplinski TJ, Tuskan GA, Yang X, Cushman JC. 2014. Engineering crassulacean acid metabolism to improve water-use efficiency. *Trends in Plant Science* **19**: 327–338.

Boxall SF, Kadu N, Dever LV, Kneřová J, Waller JL, Gould PJD, Hartwell J. 2020. *Kalanchoë* PPC1 is essential for crassulacean acid metabolism and the regulation of core circadian clock and guard cell signaling genes. *Plant Cell* **32**: 1136–1160.

Boyd RA, Gandin A, Cousins AB. 2015. Temperature responses of C_4 photosynthesis: biochemical analysis of Rubisco, phosphoenolpyruvate carboxylase, and carbonic anhydrase in *Setaria viridis*. *Plant Physiology* **169**: 1850–1861.

Brilhaus D, Bräutigam A, Mettler-Altmann T, Winter K, Weber APM. 2015. Reversible burst of transcriptional changes during induction of crassulacean acid metabolism (CAM) in *Talinum triangulare*. *Plant Physiology* **170**: 102–122.

Burgos A, Miranda E, Vilaprinyo E, Meza-Canales ID, Alves R. 2022. CAM models: lessons and implications for CAM evolution. *Frontiers in Plant Science* **13**: 893095.

von Caemmerer S. 2000. *Biochemical models of leaf photosynthesis*. Collingwood, Victoria, Australia: CSIRO Publishing.

Ceusters N, Borland AM, Ceusters J. 2021. How to resolve the enigma of diurnal malate remobilisation from the vacuole in plants with crassulacean acid metabolism? *New Phytologist* **229**: 3116–3124.

Ceusters N, Luca S, Feil R, Claes JE, Lunn JE, Van den Ende W, Ceusters J. 2019. Hierarchical clustering reveals unique features in the diel dynamics of metabolites in the CAM orchid *Phalaenopsis*. *Journal of Experimental Botany* **70**: 3269–3281.

Chaves CJN, Leal BSS, de Lemos-Filho JP. 2015. Temperature modulation of thermal tolerance of a CAM-tank bromeliad and the relationship with acid accumulation in different leaf regions. *Physiologia Plantarum* **154**: 500–510.

Cheung CM, Poolman MG, Fell DA, Ratcliffe RG, Sweetlove LJ. 2014. A diel flux balance model captures interactions between light and dark metabolism during day-night cycles in C_3 and crassulacean acid metabolism leaves. *Plant Physiology* **165**: 917–929.

Chomthong M, Griffiths H. 2020. Model approaches to advance crassulacean acid metabolism system integration. *The Plant Journal* **101**: 951–963.

Cockburn W, Ting IP, Sternberg LO. 1979. Relationships between stomatal behavior and internal carbon dioxide concentration in crassulacean acid metabolism plants. *Plant Physiology* **63**: 1029–1032.

Collatz GJ, Ribas-Carbo M, Berry J. 1992. Coupled photosynthesis-stomatal conductance model for leaves of C_4 plants. *Functional Plant Biology* **19**: 519–538.

Comins H, Farquhar G. 1982. Stomatal regulation and water economy in Crassulacean acid metabolism plants: an optimization model. *Journal of Theoretical Biology* **99**: 263–284.

Cushman JC, Davis SC, Yang X, Borland AM. 2015. Development and use of bioenergy feedstocks for semi-arid and arid lands. *Journal of Experimental Botany* **66**: 4177–4193.

Davey PA, Hunt S, Hymus GJ, DeLucia EH, Drake BG, Karnosky DF, Long SP. 2004. Respiratory oxygen uptake is not decreased by an instantaneous elevation of $[CO_2]$, but is increased with long-term growth in the field at elevated $[CO_2]$. *Plant Physiology* **134**: 520–527.

Davis SC, Kuzmick ER, Niechayev N, Hunsaker DJ. 2017. Productivity and water use efficiency of *Agave americana* in the first field trial as bioenergy feedstock on arid lands. *Global Change Biology Bioenergy* **9**: 314–325.

Davis SC, LeBauer DS, Long SP. 2014. Light to liquid fuel: theoretical and realized energyconversion efficiency of plants using crassulacean acid metabolism (CAM) in arid conditions. *Journal of Experimental Botany* **65**: 3471–3478.

Davis SC, Simpson J, Gil-Vega KC, Niechayev NA, Ev T, Castano NH, Dever LV, Búrquez A. 2019. Undervalued potential of crassulacean acid metabolism for current and future agricultural production. *Journal of Experimental Botany* **70**: 6521–6537.

De Pury DGG, Farquhar G. 1997. Simple scaling of photosynthesis from leaves to canopies without the errors of big-leaf models. *Plant, Cell & Environment* **20**: 537–557.

De Souza AP, Burguess SJ, Doran L, Hansen J, Manukyan L, Maryn N, Gotarkar D, Leonelli L, Niyogi KK, Long SP. 2022. Soybean photosynthesis and crop yield is improved by accelerating recovery from photoprotection. *Science* **377**: 851–854.

Dever LV, Boxall SF, Kneřová J, Hartwell J. 2015. Transgenic perturbation of the decarboxylation phase of Crassulacean acid metabolism alters physiology and metabolism but has only a small effect on growth. *Plant Physiology* **167**: 44–59.

Díaz-Torres JJ, Hernández-Mena L, Murillo-Tovar MA, León-Becerril E, López-López A, Suárez-Plascencia C, Aviña-Rodriguez E, Barradas-Gimate A, Ojeda-Castillo V. 2017. Assessment of the modulation effect of rainfall on solar radiation availability at the Earth's surface. *Meteorological Applications* **24**: 180–190.

Dittrich P. 1976. Nicotinamide adenine dinucleotide-specific "malic" enzyme in *Kalanchoë daigremontiana* and other plants exhibiting crassulacean acid metabolism. *Plant Physiology* **57**: 310–314.

Farquhar GD, von Caemmerer S, Berry JA. 1980. A biochemical model of photosynthetic CO_2 assimilation in leaves of C_3 species. *Planta* **149**: 78–90.

Freschi L, Takahashi CA, Cambui CA, Semprebom TR, Cruz AB, Mioto PT, de Melo VL, Calvente A, Latansio-Aidar SR, Aidar MPM. 2010. Specific leaf areas of the tank bromeliad *Guzmania monostachia* perform distinct functions in response to water shortage. *Journal of Plant Physiology* **167**: 526–533.

Garcia-Moya E, Romero-Manzanares A, Nobel PS. 2011. Highlights for *Agave* productivity. *Global Change Biology Bioenergy* **3**: 4–14.

Gentry HS. 1982. *Agaves of continental North America*. Tucson, AZ, USA: The University of Arizona Press.

Hartzell S, Bartlett MS, Inglese P, Consoli S, Yin J, Porporato A. 2021. Modelling nonlinear dynamics of Crassulacean acid metabolism productivity and water use for global predictions. *Plant, Cell & Environment* **44**: 34–48.

Hartzell S, Bartlett MS, Porporato A. 2018. Unified representation of the C_3, C_4, and CAM photosynthetic pathways with the Photo3 model. *Ecological Modelling* **384**: 173–187.

Holtum JAM, Winter K. 2014. Limited photosynthetic plasticity in the leaf-succulent CAM plant *Agave angustifolia*. *Functional Plant Biology* **41**: 843–849.

Huang J, Yu H, Guan X, Wang G, Guo R. 2016. Accelerated dryland expansion under climate change. *Nature Climate Change* **6**: 166–171.

IPCC. 2023. *IPCC Sixth Assessment Report (AR6) "climate change 2023" synthesis report approved summary for policymakers.* Geneva, Switzerland: IPCC/UNEP/WHO.

Kannan K, Wang Y, Lang M, Challa GS, Long SP, Marshall-Colon A. 2019. Combining gene network, metabolic and leaf-level models shows means to future-proof soybean photosynthesis under rising CO_2. *in silico Plants* **1**: diz008.

Kearns J, Teletzke G, Palmer J, Thomann H, Kheshgi H, Chen Y-HH, Paltsev S, Herzog H. 2017. Developing a consistent database for regional geologic CO_2 storage capacity worldwide. *Energy Procedia* **114**: 4697–4709.

Kluge M, Ting IP. 1978. *Crassulacean acid metabolism: analysis of an ecological adaptation*. Berlin, Germany: Springer-Verlag.

Köhler IH, Ruiz-Vera UM, VanLoocke A, Thomey ML, Clemente T, Long SP, Ort DR, Bernacchi CJ. 2017. Expression of cyanobacterial FBP/SBPase in soybean prevents yield depression under future climate conditions. *Journal of Experimental Botany* **68**: 715–726.

Kromdijk J, Głowacka K, Leonelli L, Gabilly ST, Iwai M, Niyogi KK, Long SP. 2016. Improving photosynthesis and crop productivity by accelerating recovery from photoprotection. *Science* **354**: 857–861.

Lim SD, Lee S, Choi W-G, Yim WC, Cushman JC. 2019. Laying the foundation for crassulacean acid metabolism (CAM) biodesign: expression of the C_4 metabolism cycle genes of CAM in Arabidopsis. *Frontiers in Plant Science* **10**: 101.

Liu D, Chen M, Mendoza B, Cheng H, Hu R, Li L, Trinh CT, Tuskan GA, Yang X. 2019. CRISPR/Cas9-mediated targeted mutagenesis for functional genomics research of crassulacean acid metabolism plants. *Journal of Experimental Botany* **70**: 6621–6629.

Lüttge U. 2000. The tonoplast functioning as the master switch for circadian regulation of crassulacean acid metabolism. *Planta* **211**: 761–769.

Lüttge U, Ball E. 1987. Dark respiration of CAM plants. *Plant Physiology and Biochemistry* **25**: 3–10.

Lüttge U, Beck F. 1992. Endogenous rhythms and chaos in crassulacean acid metabolism. *Planta* **188**: 28–38.

Lüttge U, Smith JAC. 1984. Mechanism of passive malic-acid efflux from vacuoles of the CAM plant *Kalanchoë daigremontiana*. *Journal of Membrane Biology* **81**: 149–158.

Lüttge U, Smith JAC, Marigo OCB. 1981. Energetics of malate accumulation in the vacuoles of *Kalanchoë tubiflora* cells. *FEBS Letters* **126**: 81–84.

Males J, Griffiths H. 2017. Stomatal biology of CAM plants. *Plant Physiology* **174**: 550–560.

MATLAB. 2017. Mathworks Inc. [WWW document] URL www.mathworks.com [accessed 14 April 2023].

Maxwell K, Borland AM, Haslam RP, Helliker BR, Roberts A, Griffiths H. 1999. Modulation of Rubisco activity during the diurnal phases of the crassulacean acid metabolism plant *Kalanchoë daigremontiana*. *Plant Physiology* **121**: 849–856.

Ming R, VanBuren R, Wai CM, Tang H, Schatz MC, Bowers JE, Lyons E, Wang M-L, Chen J, Biggers E *et al.* 2015. The pineapple genome and the evolution of CAM photosynthesis. *Nature Genetics* **47**: 1435–1442.

Morgan JA, Rhodes D. 2002. Mathematical modeling of plant metabolic pathways. *Metabolic Engineering* **4**: 80–89.

Morison JIL. 1987. Intercellular CO_2 concentration and stomatal response to CO_2. In: Zeiger E, Farquhar GD, Cowan IR, eds. *Stomatal function*. Stanford, CA, USA: Stanford University Press, 229–251.

Nabhan GP, Colunga-GarcíaMarín P, Zizumbo-Villarreal D. 2022. Comparing wild and cultivated food plant richness between the Arid American and the Mesoamerican centers of diversity, as means to advance indigenous food sovereignty in the face of climate change. *Frontiers in Sustainable Food Systems* **6**: 840619.

Neales T. 1973. The effect of night temperature on CO_2 assimilation, transpiration, and water use efficiency in *Agave americana* L. *Australian Journal of Biological Sciences* **26**: 705–714.

Neff R, Blasius B, Beck F, Lüttge U. 1998. Thermodynamics and energetics of the tonoplast membrane operating as a hysteresis switch in an oscillatory model of crassulacean acid metabolism. *Journal of Membrane Biology* **165**: 37–43.

Niechayev NA, Jones AM, Rosenthal DM, Davis SC. 2019a. A model of environmental limitations on production of *Agave americana* L. grown as a biofuel crop in semi-arid regions. *Journal of Experimental Botany* **70**: 6549–6559.

Niechayev NA, Pereira PN, Cushman JC. 2019b. Understanding trait diversity associated with crassulacean acid metabolism (CAM). *Current Opinion in Plant Biology* **49**: 74–85.

Nimmo HG. 2000. The regulation of phosphoenolpyruvate carboxylase in CAM plants. *Trends in Plant Science* **5**: 75–80.

Nobel PS. 1984. Productivity of *Agave deserti*: measurement by dry weight and monthly prediction using physiological responses to environmental parameters. *Oecologia* **64**: 1–7.

Nobel PS. 1985. PAR, water and temperature limitations on the productivity of cultivated *Agave fourcroydes* (henequen). *Journal of Applied Ecology* **22**: 157–173.

Nobel PS. 1988. *Environmental biology of agaves and cacti*. Cambridge, UK: Cambridge University Press.

Nobel PS. 1991. Achievable productivities of certain CAM plants: basis for high values compared with C_3 and C_4 plants. *New Phytologist* **119**: 183–205.

Nobel PS. 2000. Crop ecosystem responses to climatic change: crassulacean acid metabolism crops. In: Reddy KR, Hodges HF, eds. *Climate change and global crop productivity*. New York, NY, USA: CABI Publishing, 315–331.

Nobel PS, García de Cortázar V. 1987. Interception of photosynthetically active radiation and predicted productivity for *Agave* rosettes. *Photosynthetica* **21**: 261–272.

Nobel PS, Valenzuela AG. 1987. Environmental responses and productivity of the CAM plant, *Agave tequilana*. *Agricultural and Forest Meteorology* **39**: 319–334.

Nungesser D, Kluge M, Tolle H, Oppelt W. 1984. A dynamic computer model of the metabolic and regulatory processes in Crassulacean acid metabolism. *Planta* **162**: 204–214.

Ogburn RM, Edwards EJ. 2010. The ecological water-use strategies of succulent plants. *Advances in Botanical Research* **55**: 179–225.

Ögren E, Evans JR. 1993. Photosynthetic light-response curves. 1. The influence of CO_2 partial pressure and leaf inversion. *Planta* **189**: 182–190.

Osmond CB. 1978. Crassulacean acid metabolism: a curiosity in context. *Annual Review of Plant Physiology* **29**: 379–414.

Owen NA, Choncubhair ÓN, Males J, del Real Laborde JI, Rubio-Cortés R, Griffiths H, Lanigan G. 2016. Eddy covariance captures four-phase crassulacean acid metabolism (CAM) gas exchange signature in *Agave*. *Plant, Cell & Environment* **39**: 295–309.

Owen NA, Griffiths H. 2013. A system dynamics model integrating physiology and biochemical regulation predicts extent of crassulacean acid metabolism (CAM) phases. *New Phytologist* **200**: 1116–1131.

Owen NA, Griffiths H. 2014. Marginal land bioethanol yield potential of four crassulacean acid metabolism candidates (*Agave fourcroydes*, *Agave salmiana*, *Agave tequilana* and *Opuntia ficus-indica*) in Australia. *Global Change Biology Bioenergy* **6**: 687–703.

Pérez-Pimienta JA, López-Ortega MG, Sanchez A. 2017. Recent developments in agave performance as a drought-tolerant biofuel feedstock: agronomics, characterization, and biorefining. *Biofuels, Bioproducts and Biorefining* **11**: 732–748.

Popp M, Janett HP, Lüttge U, Medina E. 2003. Metabolite gradients and carbohydrate translocation in rosette leaves of CAM and C_3 bromeliads. *New Phytologist* **157**: 649–656.

Prăvălie R. 2016. Drylands extent and environmental issues. A global approach. *Earth-Science Reviews* **161**: 259–278.

Purseglove J. 1972. *Tropical crops. Monocotyledons 1*. London, UK: Longman.

Renewable Fuels Association. 2021. [WWW document] URL https://ethanolrfa.org/markets-and-statistics/annual-ethanol-production [accessed 14 March 2023].

Saitou K, Agata W, Asakura M, Kubota F. 1992. Structural and kinetic properties of NADP-malic enzyme from the inducible Crassulacean Acid Metabolism plant *Mesembryanthemum crystallinum* L. *Plant and Cell Physiology* **33**: 595–600.

Schiller K, Bräutigam A. 2021. Engineering of crassulacean acid metabolism. *Annual Review of Plant Biology* **72**: 77–103.

Shameer S, Baghalian K, Cheung CYM, Ratcliffe RG, Sweetlove LJ. 2018. Computational analysis of the productivity potential of CAM. *Nature Plants* **4**: 165–171.

Shameer S, Wang Y, Bota P, Ratcliffe RG, Long SP, Sweetlove LJ. 2022. A hybrid kinetic and constraint-based model of leaf metabolism allows predictions of metabolic fluxes in different environments. *The Plant Journal* **109**: 295–313.

Slattery RA, Ort DR. 2015. Photosynthetic energy conversion efficiency: setting a baseline for gauging future improvements in important food and biofuel crops. *Plant Physiology* **168**: 383–392.

Smith JAC, Ingram J, Tsiantis MS, Barkla BJ, Bartholomew DM, Bettey M, Pantoja O, Pennington AJ. 1996. Transport across the vacuolar membrane in CAM plants. In: Winter K, Smith JAC, eds. *Crassulacean acid metabolism: biochemistry, ecophysiology and evolution.* Berlin, Germany: Springer, 53–71.

Smith JAC, Nobel PS. 1986. Water movement and storage in a desert succulent: anatomy and rehydration kinetics for leaves of *Agave deserti*. *Journal of Experimental Botany* **37**: 1044–1053.

Song Q, Zhang GL, Zhu X-G. 2013. Optimal crop canopy architecture to maximise canopy photosynthetic CO_2 uptake under elevated CO_2 – a theoretical study using a mechanistic model of canopy photosynthesis. *Functional Plant Biology* **40**: 109–124.

Spalding MH, Stumpf DK, Ku MSB, Burris RH, Edwards GE. 1979. Crassulacean acid metabolism and diurnal variations of internal CO_2 and O_2 concentrations in *Sedum praealtum* DC. *Australian Journal of Plant Physiology* **6**: 557–567.

Stewart JR. 2015. *Agave* as a model CAM crop system for a warming and drying world. *Frontiers in Plant Science* **6**: 684.

Töpfer N, Braam T, Shameer S, Ratcliffe RG, Sweetlove LJ. 2020. Alternative crassulacean acid metabolism modes provide environment-specific water-saving benefits in a leaf metabolic model. *Plant Cell* **32**: 3689–3705.

Van Velthuizen H. 2007. *Mapping biophysical factors that influence agricultural production and rural vulnerability (no. 11)*. Rome, Italy: Food & Agriculture Organization.

Wai CM, VanBuren R, Zhang J, Huang L, Miao W, Edger PP, Yim WC, Priest HD, Meyers BC, Mockler T *et al.* 2017. Temporal and spatial transcriptomic and microRNA dynamics of CAM photosynthesis in pineapple. *The Plant Journal* **92**: 19–30.

Wang Y, Bräutigam A, Weber APM, Zhu X-G. 2014a. Three distinct biochemical subtypes of C_4 photosynthesis? A modelling analysis. *Journal of Experimental Botany* **65**: 3567–3578.

Wang Y, Chan KX, Long SP. 2021. Towards a dynamic photosynthesis model to guide yield improvement in C_4 crops. *The Plant Journal* **107**: 343–359.

Wang Y, Long SP, Zhu X-G. 2014b. Elements required for an efficient NADP-malic enzyme type C_4 photosynthesis. *Plant Physiology* **164**: 2231–2246.

Wang Y, Song Q, Jaiswal D, De Souza AP, Long SP, Zhu XG. 2017. Development of a three-dimensional ray-tracing model of sugarcane canopy photosynthesis and its application in assessing impacts of varied row spacing. *Bioenergy Research* **10**: 626–634.

Winter K. 1985. Crassulacean acid metabolism. In: Barber J, Baker NR, eds. *Photosynthetic mechanisms and the environment.* Amsterdam, the Netherlands: Elsevier, 329–387.

Winter K, Garcia M, Holtum JAM. 2014. Nocturnal versus diurnal CO_2 uptake: how flexible is *Agave angustifolia*? *Journal of Experimental Botany* **65**: 3695–3703.

Winter K, Smith JAC. 1996. Crassulacean acid metabolism: current status and perspectives. In: Winter K, Smith JAC, eds. *Crassulacean acid metabolism: biochemistry, ecophysiology and evolution.* Berlin, Germany: Springer-Verlag, 389–426.

Winter K, Smith JAC. 2022. CAM photosynthesis: the acid test. *New Phytologist* **233**: 599–609.

Woodhouse RM, Williams JG, Nobel PS. 1980. Leaf orientation, radiation interception, and nocturnal acidity increases by the CAM plant *Agave deserti* (Agavaceae). *American Journal of Botany* **67**: 1179–1185.

Yan X, Corbin KR, Burton RA, Tan DK. 2020. Agave: a promising feedstock for biofuels in the water-energy-food-environment (WEFE) nexus. *Journal of Cleaner Production* **261**: 121283.

Yan X, Tan DK, Inderwildi OR, Smith JAC, King DA. 2011. Life cycle energy and greenhouse gas analysis for *Agave*-derived bioethanol. *Energy & Environmental Science* **4**: 3110–3121.

Yang X, Cushman JC, Borland AM, Edwards EJ, Wullschleger SD, Tuskan GA, Owen NA, Griffiths H, Smith JAC, De Paoli HC *et al.* 2015. A roadmap for research on crassulacean acid metabolism (CAM) to enhance sustainable food and bioenergy production in a hotter, drier world. *New Phytologist* **207**: 491–504.

Yang X, Hu R, Yin H, Jenkins J, Shu S, Tang H, Liu D, Weighill DA, Cheol Yim W, Ha J *et al.* 2017. The *Kalanchoë* genome provides insights into convergent evolution and building blocks of crassulacean acid metabolism. *Nature Communications* **8**: 1899.

Zhu XG, de Sturler E, Long SP. 2007. Optimizing the distribution of resources between enzymes of carbon metabolism can dramatically increase photosynthetic rate: a numerical simulation using an evolutionary algorithm. *Plant Physiology* **145**: 513–526.

Zhu XG, Long SP, Ort DR. 2008. What is the maximum efficiency with which photosynthesis can convert solar energy into biomass? *Current Opinion in Biotechnology* **19**: 153–159.

Zhu XG, Ort DR, Whitmarsh J, Long SP. 2004. The slow reversibility of photosystem II thermal energy dissipation on transfer from high to low light may cause large losses in carbon gain by crop canopies: a theoretical analysis. *Journal of Experimental Botany* **55**: 1167–1175.

Supporting Information

Additional Supporting Information may be found online in the Supporting Information section at the end of the article.

Fig. S1 Deriving the energy cost of the NAD(P)-ME type CAM pathway.

Fig. S2 Energy cost of the PEPCK-type CAM pathway.

Fig. S3 Daily change of leaf carbon gain in various light conditions.

Fig. S4 Theoretical maximal photosynthetic conversion efficiency of plants from interception of radiation to the formation of biomass.

Fig. S5 Sensitivity analysis of the simulated diurnal photosynthetic CO_2 uptake rate of an *Agave tequilana* leaf.

Fig. S6 Predicted daily carbohydrate mass gain and water use efficiency (WUE) of *Agave tequilana* canopy (1-yr-old plant).

Fig. S7 Predicted daily carbohydrate mass gain and WUE of *Agave tequilana* canopy (3-yr-old plant).

Fig. S8 Predicted daily carbohydrate mass gain and WUE of *Agave tequilana* canopy (6-yr-old plant).

Fig. S9 Impact of varying leaf area index (LAI), maximum leaf angle and leaf reflectance on agave plant daily net CO_2 uptake WUE.

Fig. S10 Simulated diel changes in stomatal conductance (g_s).

Fig. S11 Influence of leaf shape on light absorption.

Fig. S12 Simulated diel changes in net leaf CO_2 uptake and the carboxylation and oxygenation rate by Rubisco.

Methods S1 Canopy CO_2 assimilation prediction.

Methods S2 Metabolic model equations and parameters.

Methods S3 Maximum energy conversion efficiency of the CAM pathway.

Please note: Wiley is not responsible for the content or functionality of any Supporting Information supplied by the authors. Any queries (other than missing material) should be directed to the *New Phytologist* Central Office.